

Dynamic Quantum Tunneling in Mesoscopic Driven Duffing Oscillators

Lingzhen Guo, Zhigang Zheng, and Xin-Qi Li

Department of Physics, Beijing Normal University, Beijing 100875, China

YiJing Yan

Department of Chemistry, Hong Kong University of Science and Technology, Kowloon, Hong Kong

(Dated: June 1, 2010)

We show that a mesoscopic driven Duffing oscillator exhibits dynamic quantum tunneling between two attractors. In addition to an induced quantum shift of the bifurcation point, the *mesoscopic* nature also results in a new scaling exponent with the driving distance.

PACS numbers: 05.45.-a, 85.25.Cp, 03.65.Yz, 74.50.+r

In the light of nanomechanics [1] and as a qubit readout device for superconducting qubits (i.e., the Josephson bifurcation amplifier) [2–5], the quantum properties of the driven Duffing oscillator (DDO) gained renewed interest in the past years [6–11]. For instance, the quantum signature in the bistable region of a DDO was analyzed, based on simulating a Lindblad-type master equation and comparing the Wigner function with classical probability distribution in phase space [6]. In terms of amplitude and phase responses to the driving frequency, quantum behaviors of DDO such as resonant tunneling and photon-assisted tunneling were also discussed [7]. Moreover, in Ref. [8–10], the switching rate between the bistable states near the bifurcation point, due to quantum and/or thermal fluctuations, was estimated by means of the WKB theory or semiclassical methods such as the mean-first-passage-time approach.

In this work we consider a *mesoscopic* DDO, which involves more than ten levels in the nonlinear dynamics, being interestingly between the quantum few-level and the classical dense-level (or continuum) limit. In this regime, quantum effect is crucially important. We will focus on the dynamic quantum tunneling between two attractors in the bistable region, in particular account for a quantum shift of the bifurcation point associated with the *mesoscopic* nature, and extract a new scaling exponent with the driving distance.

Model and Qualitative Considerations.— The Duffing oscillator in the presence of driving is described by

$$H_S(t) = p^2/2m + m\Omega^2 x^2/2 - \gamma x^4 + F(t)x. \quad (1)$$

Related to the Josephson bifurcation amplifier (JBA), $F(t) = 2F_0 \cos(\nu t)$ describes the microwave driving; and noticeably, the driving frequency should satisfy $\nu < \Omega$. Other parameters associated with the JBA circuit read: $m = (\hbar/2e)^2 C$, $\Omega = \sqrt{2eI_c/(\hbar C)}$, $F_0 = \hbar I/(2e)$, and $\gamma = m\Omega^2/24$; with C the capacitance of the Josephson junction, I_c the critical current, and I the driving current. In this context, x denotes the phase difference across the Josephson junction. In addition, the Duffing oscillator is affected by environment, which together with the coupling can be modelled as $H_E = \sum_i (m_i \omega_i^2 x_i^2/2 + p_i^2/2m_i)$ and $H_I = -x \sum_i \lambda_i x_i$. Typically, the spectral density of the bath, $J(\omega) = \pi \sum_i \lambda_i^2 \delta(\omega - \omega_i)/(2m_i \omega_i)$, in Ohmic case reads

$J(\omega) = m\kappa\omega \exp(-\omega/\omega_c)$, with κ the friction coefficient, and ω_c the high frequency cutoff. For later use, we also introduce $b = \sum_i \lambda_i b_i / \sqrt{2}$, with $b_i = (m_i \omega_i x_i + i p_i) / \sqrt{2m_i \hbar \omega_i}$.

Notice that the Duffing oscillator described by Eq. (1) has only finite number of bound states. In the absence of external driving, this becomes clear from the potential profile, $V(x) = \frac{m\Omega^2}{2}x^2 - \gamma x^4$, which defines a single well with identical barrier height $V_0 = m^2\Omega^4/(16\gamma)$ at $x = \pm \sqrt{m\Omega^2/(4\gamma)}$. As a rough estimate, the number of bound states is the ratio of V_0 and $\hbar\Omega$, which gives $N = \frac{m^2\Omega^4}{16\gamma\hbar\Omega} = \frac{m\Omega}{16\hbar\tilde{\gamma}} = \frac{\aleph}{16\tilde{\gamma}}$. We will see later that $\aleph \equiv m\Omega/\hbar$ defined here is a useful characteristic quantity. We also introduced a reduced nonlinear coefficient, $\tilde{\gamma} = \gamma/(m\Omega^2)$. In our model, $\gamma = m\Omega^2/24$, so approximately the number of bound states is $3\aleph/2$. In the experiment of Ref. [2], $\aleph \approx 366$, which implies a classical DDO. In the present work, however, we are interested in a *mesoscopic* regime, thus assuming possible parameters $I_c = 39\text{nA}$, $C = 0.91\text{pF}$, $\kappa = 0.01\Omega$, and $\omega_c = 10\Omega$. Accordingly, $\aleph \approx 12$. Also, we assume an experimentally accessible temperature of 5 mK.

Now we present a qualitative understanding to the driving dynamics of DDO, respectively, in the laboratory frame and in a rotating frame. In Fig. 1(a) we show the energy level diagram of the Duffing oscillator in the absence of driving. To the second-order perturbation of the quartic potential, the energy level reads

$$E_n = \left[n + \frac{1}{2} - \frac{3\tilde{\gamma}(2n^2 + 2n + 1)}{4\aleph} \right] \hbar\Omega. \quad (2)$$

Accordingly, the adjacent level spacing, $\Delta E_n = E_n - E_{n-1} = (1 - 3\tilde{\gamma}n/\aleph)\hbar\Omega$, decreases with n . This property, together with a negative frequency detuning (e.g. $\delta = 1 - \nu/\Omega = 0.065$ in later simulation), would result in the bistability behavior. Qualitatively speaking, for weak driving, the oscillator will largely remain in the initial ground state; for stronger driving, however, it will be increasingly excited to high energy states around n^* , roughly determined by $\hbar\nu = \Delta E_{n^*}$, leading to $n^* = \aleph\delta/(3\tilde{\gamma})$.

We notice that an alternative (a better) way to inspect the quantum dynamics is in a rotating frame with the driving frequency ν , where the driving field becomes time independent.

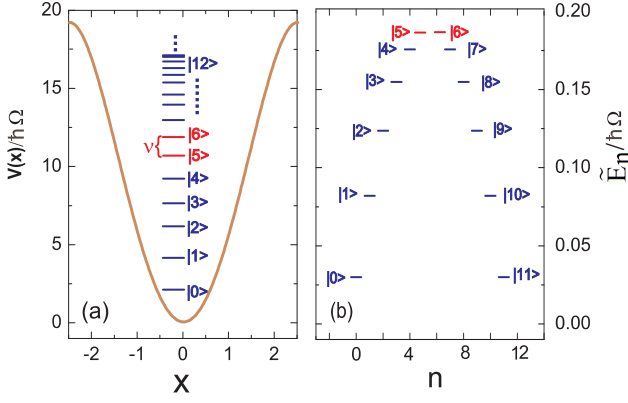


FIG. 1: Energy diagram of the non-driven Duffing oscillator in (a) the laboratory frame, and (b) the rotating frame.

This can be implemented by applying a rotating transformation $U(t) = \exp\{-ivta^\dagger a\}$, where a (a^\dagger) is the annihilation (creation) operator of the DDO. Dropping fast rotating terms, i.e., under the rotating wave approximation (RWA), we obtain

$$\tilde{H}_S = \delta \left(\frac{p^2}{2m} + \frac{1}{2}m\Omega^2 x^2 \right) - \frac{6\gamma}{4m^2\Omega^4} \left(\frac{p^2}{2m} + \frac{1}{2}m\Omega^2 x^2 \right)^2 + F_0 x. \quad (3)$$

In the absence of driving, this rotated Hamiltonian is naturally diagonal, with the eigenstates of harmonic oscillator ψ_n , and eigenvalues

$$\tilde{E}_n = \left[n + \frac{1}{2} - \frac{3\tilde{\gamma}}{2\mathfrak{N}\delta} \left(n + \frac{1}{2} \right)^2 \right] \hbar\delta\Omega, \quad (4)$$

as schematically shown in Fig. 1(b). Interestingly, we find here that the n^* th level is the highest one (noting that n^* labels the resonance level-pair in the laboratory frame). Also, the level spacing in the rotating frame is much smaller than its counterpart in the laboratory frame. Then, it is clear that the DDO's dynamics in this rotating frame is governed by the interplay of $F_0 x$ -induced transition and environmental dissipation. More interestingly, in the presence of $F_0 x$, we can diagonalize the transformed Hamiltonian \tilde{H}_S of Eq. (3) and denote the eigenstates by $\tilde{\psi}_n$. It is found that a one-to-one correspondence exists between ψ_n and $\tilde{\psi}_n$, which can be understood in the spirit of adiabatic switching. Then, $\tilde{\psi}_{n^*}$ and $\tilde{\psi}_0$ can be analogously regarded as two *attractors*, which direct the evolution, determine the final state, and are responsible to a bistability behavior. In the remained part of this work, the two attractors will be termed also as small amplitude state (SAS) and large amplitude state (LAS).

Master Equation in Rotating Frame.— Following Ref. [12], in laboratory frame as usual, a weakly damped DDO can be well described by the master equation for its reduced density matrix:

$$\dot{\rho}(t) = -i\hbar^{-1} \mathcal{L}_S \rho(t) - \hbar^{-2} \int_0^t d\tau \langle \mathcal{L}_I(t) \mathcal{G}(t, \tau) \mathcal{L}_I(\tau) \mathcal{G}^\dagger(t, \tau) \rangle \rho(t). \quad (5)$$

Here $\mathcal{L}_S(\dots) = [H_S, (\dots)]$ is associated with the DDO Hamiltonian in laboratory frame, while $\mathcal{G}(t, \tau)(\dots) = G(t, \tau)(\dots)G^\dagger(t, \tau)$ is the relevant propagator in Liouvillian space, with $G(t, \tau)$ the usual Green's function given by H_S . The interaction Liouvillian superoperator \mathcal{L}_I is defined by $\mathcal{L}_I(\dots) = [H_I, (\dots)]$, where $H_I = -x \sum_j \lambda_j x_j \equiv -x X_E$ describes the coupling of DDO to environment. The average in Eq. (5) means $\langle (\dots) \rangle = \text{tr}_E[(\dots)\rho_E]$, with ρ_E the thermal equilibrium density operator of the environment. In laboratory frame, the driving in H_S is time-dependent, which would complicate the dissipation terms in Eq. (5) and make the numerical simulation difficult. To overcome this difficulty, we transform Eq. (5) into the rotating frame

$$\dot{\tilde{\rho}}(t) = -i\hbar^{-1} \tilde{\mathcal{L}}_S \tilde{\rho}(t) - \hbar^{-2} \int_0^t d\tau \langle \tilde{\mathcal{L}}_I(t) \tilde{\mathcal{G}}(t, \tau) \tilde{\mathcal{L}}_I(\tau) \tilde{\mathcal{G}}^\dagger(t, \tau) \rangle \tilde{\rho}(t). \quad (6)$$

The various transformed quantities are defined here as: $\tilde{\rho}(t) = U^\dagger \rho(t) U$, $\tilde{\mathcal{L}}_S(\dots) = [U^\dagger H_S U + i\hbar U^\dagger \dot{U}, (\dots)] = [\tilde{H}_S, (\dots)]$, $\tilde{\mathcal{L}}_I(\dots) = [U^\dagger H_I U, (\dots)] = [\tilde{H}_I, (\dots)]$, and $\tilde{\mathcal{G}}(t, \tau)$ is the propagator associated with \tilde{H}_S . Note that in the rotating frame the coupling Hamiltonian becomes time dependent, i.e., $\tilde{H}_I = -U^\dagger x U X_E = -\sqrt{\hbar/2m\Omega}(a^\dagger e^{ivt} + a e^{-ivt})X_E$. Inserting this result into Eq. (6) yields

$$\begin{aligned} \dot{\tilde{\rho}}(t) = & -i\hbar^{-1} \tilde{\mathcal{L}}_S \tilde{\rho}(t) - \frac{1}{4\mathfrak{N}} \{ [a^\dagger, (C(-\tilde{\mathcal{L}}_S + \nu)a)\tilde{\rho}] \\ & + [a, (C(-\tilde{\mathcal{L}}_S - \nu)a^\dagger)\tilde{\rho}] + e^{i2\nu t} [a^\dagger, (C(-\tilde{\mathcal{L}}_S - \nu)a^\dagger)\tilde{\rho}] \\ & + e^{-i2\nu t} [a, (C(-\tilde{\mathcal{L}}_S + \nu)a)\tilde{\rho}] + \text{H.c.} \}. \end{aligned} \quad (7)$$

In deriving this result, the established Markov-Redfield approximation has been applied. Accordingly, the spectral function, $C(\tilde{\mathcal{L}}_S)$, is a Fourier transform of the environment correlator: $C(\tilde{\mathcal{L}}_S) = \int_{-\infty}^{+\infty} dt C(t) e^{i\hbar^{-1} \tilde{\mathcal{L}}_S t}$, and $C(t) = \text{Tr}_E[X_E(t)X_E(0)\rho_E]$.

Eq. (7) is the desired equation we obtain in the rotating frame, on which our numerical simulation will be based. To relate it with other work, we first drop the fast oscillating terms in Eq. (7) under the rotating wave approximation. Then, we assume further a *harmonic* approximation: $\tilde{\mathcal{L}}_S a \approx -\hbar\delta\Omega a$, and $\tilde{\mathcal{L}}_S a^\dagger \approx \hbar\delta\Omega a^\dagger$. As a result, the well-known Lindblad-type master equation is obtained:

$$\dot{\tilde{\rho}}(t) = -i\hbar^{-1} \tilde{\mathcal{L}}_S \tilde{\rho}(t) + \kappa \{ [1 + n(\Omega)] \mathcal{D}[a] \tilde{\rho} + n(\Omega) \mathcal{D}[a^\dagger] \tilde{\rho} \}, \quad (8)$$

where the Lindblad superoperator is defined through $\mathcal{D}[A]\tilde{\rho} \equiv A\tilde{\rho}A^\dagger - \frac{1}{2}\{A^\dagger A, \tilde{\rho}\}$. In obtaining Eq. (8), the explicit form of the spectral function has been used, i.e., $C(\omega) = 2[1 + n(\omega)]J(\omega)$, where $n(\omega)$ is the Bose function. We notice that in Ref. [9] the study of quantum activation in this same system was based on Eq. (8), together also with a few techniques and approximations in later analysis.

Quantum Shift of Bifurcation Point.— For comparative purpose, we first outline the result from a classical analysis. It is well known that the classical DDO obeys [4]:

$m\ddot{x} + m\Omega^2 x + m\kappa\dot{x} - 4\gamma x^3 = -F(t)$. Define dimensionless variables $\tau = \Omega t$, $w = \nu/\Omega$, $f = \sqrt{4\gamma/(m^3\Omega^6)}2F_0$, $Q = \Omega/\kappa$, and $\Delta = -2Q\delta$; and introduce rotating transformation $x(\tau) = [\tilde{x}(\tau)e^{i\nu\tau}/2 + c.c.]/\sqrt{4\gamma/(m\Omega^2)}$. Then the slowly varying amplitude $\tilde{x}(\tau)$ of the DDO in the rotating frame satisfies the following equation of motion (EOM) [4]

$$2i\frac{d\tilde{x}}{d\tau} = \left[\frac{\Delta - i}{Q} + \frac{3}{4}|\tilde{x}|^2 \right] \tilde{x} - f. \quad (9)$$

Stationary solution of this equation yields a bistability diagram as shown in Fig. 2(a). Moreover, two critical driving strengths, $f_{B,\bar{B}}(\Delta)$ and $f_{\bar{B},B}(\Delta)$, can be obtained in the limit $Q \gg 1$:

$$f_{B,\bar{B}}(\Delta) = \frac{\Delta^{3/2}}{2\Delta_c^{3/2}} \left[1 + 3\frac{\Delta_c^2}{\Delta^2} \pm \left(1 - \frac{\Delta_c^2}{\Delta^2} \right)^{3/2} \right]^{1/2} f_c, \quad (10)$$

where $\Delta_c = -\sqrt{3}$, and $f_c = 2^{5/2}/(3^{5/4}\sqrt{\Delta^3})$. Accordingly, after restoring dimensional units, the critical driving strengths read $F_{B,\bar{B}} = \sqrt{m^3\Omega^6/(16\gamma)}f_{B,\bar{B}}$. In what follows, we will focus on the most important upper point F_B , which is to be re-denoted as F_c and taken as the unit of the driving force.

Unfortunately, in *mesoscopic* regime, as we will see later, the critical driving strength F_c determined above does not match the result from numerical simulation. It would thus be desirable to develop a *quantum* version of Eq. (9), in order to reach consensus with the direct numerical simulation. Following Ref. [13], given that the reduced density matrix satisfies the Lindblad master equation (8), in Heisenberg picture the operator a should obey an equation of motion as follows

$$\dot{a}(t) = -i\hbar^{-1}[a, \tilde{H}_S] + \kappa\tilde{D}[a]a = -i\hbar^{-1}[a, \tilde{H}_S] - \frac{\kappa}{2}a, \quad (11)$$

where the *dual*-Lindblad superoperator is defined through $\tilde{D}[A]a \equiv A^\dagger a A - \frac{1}{2}\{A^\dagger A, a\}$. Here we assumed the low temperature limit $n(\Omega) \ll 1$. Moreover, below F_c and starting with a small-amplitude state, the subsequent evolution will largely remain in a coherent state. Then, in coherent state representation and relating the coherence number $\alpha(\tau)$ with a complex amplitude $\tilde{x}(\tau) = \sqrt{8\gamma/(m\Omega^2)}\alpha^*(\tau)/\sqrt{n}$, from Eq. (11) we obtain the same EOM as Eq. (9) for $\tilde{x}(\tau)$, but with a quantum mechanically shifted detuning

$$\tilde{\Delta} = -2Q(\delta - 3\tilde{\gamma}/\aleph), \quad (12)$$

instead of the *classical* result $\Delta = -2Q\delta$. In classical case, \aleph is large, e.g., $\aleph \approx 366$ as we estimated from the experimental circuit parameters, which makes the quantum shift negligibly small. Nevertheless, in mesoscopic regime, e.g., $\aleph \approx 12$ in our case, this quantum shift is remarkably large, as shown in Fig. 2(b) and (c), where the critical driving strength moves to $0.77F_c$. Below we illustrate the quantum shift in phase space in terms of the Wigner function representation.

The Wigner function is defined as: $W(x, p, t) = 1/(\pi\hbar) \int_{-\infty}^{+\infty} \langle x + x' | \rho(t) | x - x' \rangle \exp(-i2px'/\hbar) dx'$. In Fig. 3(a)

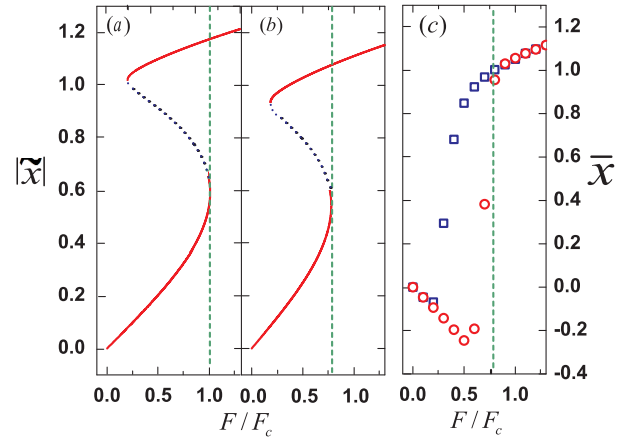


FIG. 2: (a) and (b): Bifurcation diagram of the DDO based on Eq. (9), (a) without and (b) with accounting for the quantum shift of the effective detuning [see Eq. (12)]. The dashed vertical lines indicate the respective bifurcation points. (c): Results from numerical simulation of $\bar{x}(t) = \text{Tr}[x\tilde{\rho}(t)]$ based on Eq. (7). We choose the $\bar{x}(t)$ at $t = 160 * (2\pi/\Omega)$ to represent the steady state amplitude \bar{x} . The circles and squares stand for results from different initial conditions (i.e. the SAS and LAS), from which we observe the hysteresis behavior. Here, again, the dashed vertical line indicates the bifurcation point in (b), say, $0.77F_c$ which agrees well with the numerical simulation. Parameters: $\kappa = 0.01$, $T = 5\text{mK}$, $\delta = 0.065$, $\aleph = 12$.

and (b), for comparative purpose, we plot the Wigner function simply using $\tilde{\rho}_s \equiv |\alpha\rangle\langle\alpha|$, where the coherence number α is determined from \tilde{x} , based on the steady-state solution of the amplitude EOM without and with accounting for the quantum shift, while in Fig. 3(c) and (d) we show the results from direct simulation. We see that in mesoscopic regime it is essential to account for the quantum shift, in order to make the amplitude EOM agree with numerical simulation, as indicated by the dashed vertical lines in Fig. 3. (The vertical line in each sub-figure indicates the valid “ x ” center of Wigner function of the SAS.) It is then observed that the classical result in Fig. 3(a) has considerable deviation. Moreover, from Fig. 3(d) we get an insight that starting on from certain transient stage, the oscillator evolves into a mixed state, which can be formally expressed as

$$W(x, p, t) = P_S(t)W_S(x, p) + P_L(t)W_L(x, p, t). \quad (13)$$

Here, $W_S(x, p)$ and $W_L(x, p, t)$ are the Wigner functions of the intrinsic SAS and LAS, say, the two attractors, while $P_S(t)$ and $P_L(t)$ are the respective occupation probabilities.

Tunneling Rate and Scaling Exponent.—Based on the state structure of Eq. (13), we formulate a way to determine the dynamic tunneling rate from SAS to LAS as follows. Originally, in laboratory frame, this rate can be extracted from the occupation probability of the SAS via $\Gamma_t = -dP_S(t)/dt$, while $P_S(t) = \langle \alpha e^{i\nu t} | \rho(t) | \alpha e^{i\nu t} \rangle$. Note that here we use the fact that the SAS in laboratory frame is a *rotating* coherent state. More conveniently, transformed to the rotating frame, $P_S(t) = \text{Tr}[\tilde{\rho}_s \tilde{\rho}(t)]$, where $\tilde{\rho}_s \equiv U^\dagger(t)\rho_s(t)U(t) = |\alpha\rangle\langle\alpha|$ is

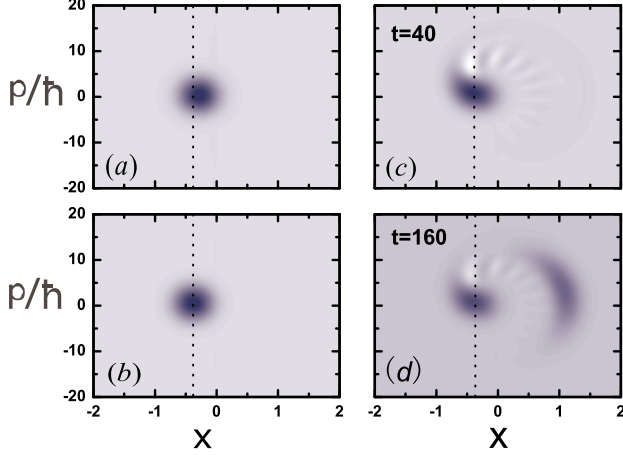


FIG. 3: (a) and (b): Wigner function of the coherent state determined from the steady-state solution of Eq. (9), (a) without and (b) with accounting for the quantum shift. (c) and (d): Wigner function from numerical simulation based on Eq. (7), at $t = 40 * (2\pi/\Omega)$ and $160 * (2\pi/\Omega)$, respectively. The dashed vertical line in each sub-figure indicates the valid “x” center of Wigner function of the SAS. Parameters: $\kappa = 0.01$, $T=5\text{mK}$, $\delta = 0.065$, $\aleph = 12$, and $F_0 = 0.7F_c$.

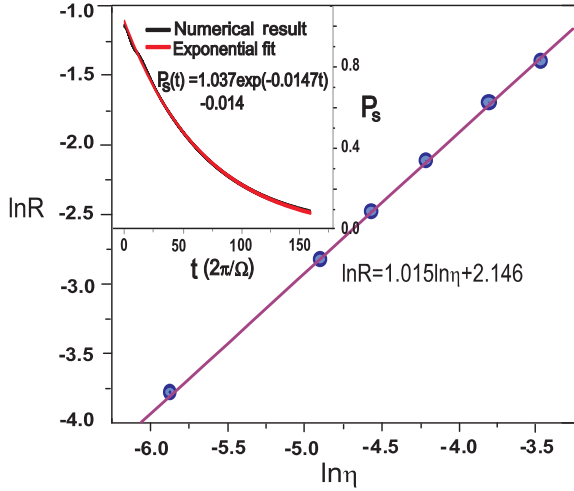


FIG. 4: Scaling behavior of the dynamic quantum tunneling rate with the driving distance to the shifted bifurcation point, say, $\eta = (0.77F_c)^2 - F_0^2$. Here, the circles are result from numerical simulation, while the linear fit gives $\alpha = 1.015$ for the tunneling action $R \propto \eta^\alpha$. Inset: an illustrative example of exponential fitting for the occupation probability of the SAS, under driving $F_0 = 0.76F_c$. Parameters: $\kappa = 0.01$, $T=5\text{mK}$, $\delta = 0.065$, and $\aleph = 12$.

static, and $\tilde{\rho}(t) = U^\dagger(t)\rho(t)U(t)$ is the DDO state in the rotating frame described by Eq. (7).

In the inset of Fig. 4 we show a representative $P_S(t)$, obtained from numerical simulation using Eq. (7) and the formalism outlined above, from which we see that a single exponential fit can well characterize $P_S(t)$. This indicates nothing

but a rate process from SAS to LAS. Moreover, the success of a single exponential fit indicates a dominant forward process from SAS to LAS. That is, at the early escape stage, the backward process from LAS to SAS is largely not happening. This is similar to the situation in determining the tunneling rate in double-well problem, where the backward tunneling process is negligibly small at certain early time stage.

Therefore, using this numerical approach we can extract the dynamic tunneling rate (Γ_t) from SAS to LAS. Further, following Ref. [9], we assume $\Gamma_t = Ce^{-R/\lambda}$. In this proposed formula, C is an irrelevant prefactor, while the exponential factor $e^{-R/\lambda}$ originates from an *effective* activation process. In limiting cases, such as for classical thermal activation, R is the activation energy and λ the temperature; while for quantum tunneling through a barrier, R is the tunneling action and λ the Planck constant. In our present case, it is a generalization, i.e., dynamic-quantum-tunneling dominated but also thermal-activation involved. So, we may view R as an effective activation energy and λ an effective Planck constant or temperature.

Very interestingly, it was found in Ref. [9] that the dynamic tunneling action R displays a perfect scaling behavior with the driving distance to the critical point, which is defined as $\eta = F_c^2 - F_0^2$. Quantitatively, it was found $R \propto \eta^\alpha$ and $\alpha = 3/2$. Now, for the mesoscopic DDO under consideration, owing to the quantum shift of the critical point, which moves to $0.77F_c$ under the assumed parameter condition as shown in Fig. 2, we thus define the driving distance by $\eta = (0.77F_c)^2 - F_0^2$. Remarkably, for the mesoscopic DDO, in Fig. 4 we demonstrate by the present precise numerical simulation that the scaling behavior of $R \propto \eta^\alpha$ still exists, yet with an alternative scaling exponent of $\alpha \simeq 1$, in stead of $\alpha = 3/2$ as found by Dykman [9].

We noticed that in Ref. [14], scaling behavior of the transition rate with the driving *frequency* (but not the driving *strength*) was analyzed to give $\alpha \simeq 1.3 \sim 1.4$, by a rough fitting from a few experimental data. Meanwhile, in the experiments by Siddiqi *et al.* [15], an effective potential with a barrier height scaled as $\Delta U_{dyn}^0 \propto [1 - (F_0/F_c)^2]^{3/2}$, was employed to analyze their measured data by means of the thermal-activation rate $\propto \exp(-\Delta U_{dyn}^0/k_B T)$. This would result in a scaling exponent of $\alpha = 3/2$. However, based on this same effective potential, a rough WKB estimate is seemingly to give a smaller scaling exponent. That is, from the quantum tunneling rate $\propto \exp(-\sqrt{\Delta U_{dyn}^0} a/\hbar)$, where a is an effective width of the barrier, one then obtains $\alpha = 3/4$.

Very recently, we performed a real time simulation for the quantum dynamics of the mesoscopic DDO directly in laboratory frame [16], where the driving field was not taken into account in the dissipation terms. In that study, similar scaling behavior with almost the same scaling exponent (i.e. $\alpha \simeq 1$) was found. In the present study, more rigorous treatment for the driving field was carried out through the rotating transformation, which enables to fully account for the driving in the dissipation terms. Moreover, we also highlighted the quantum shift of the critical driving strength in the mesoscopic regime,

in Ref. [16] which was accidentally canceled (in numerical simulation) owing to the extra term “ $x^2 \sum_i \lambda_i^2 / (2m_i \omega_i^2)$ ” in the so called Caldeira-Legget model. Quite desirably, however, both studies of Ref. [16] and the present one give consistent result. This strongly implies that the scaling exponent $\alpha = 3/2$ is non-universal, and $\alpha = 1$ is an alternate scaling exponent in the mesoscopic regime. Further investigation for the dynamic quantum tunneling behavior of DDO from a mesoscopic to the usual classical regime is extremely important, despite the greatly increasing complexity in real time simulation. This will be the task of our forthcoming research.

To summarize, in a mesoscopic regime we investigated the dynamic quantum tunneling of the driven Duffing oscillator. Owing to the mesoscopic nature, we found that the critical driving strength has a quantum shift, and the tunneling action (exponentially extracted from the tunneling rate) exhibits a perfect linear scaling behavior with the driving distance to the quantum shifted critical point.

Acknowledgements.— This work was supported by the National Natural Science Foundation of China (No. 10874176, 10875011 and 10575010), the Major State Basic Research Project (No. 2006CB921201), and the Foundation of Doctoral Training (No. 20060027009).

- [2] I. Siddiqi *et al.*, Phys. Rev. Lett. **84**, 207002 (2004); I. Siddiqi *et al.*, Phys. Rev. Lett. **94**, 027005 (2005).
- [3] I. Siddiqi *et al.*, Phys. Rev. B **73**, 054510 (2006).
- [4] V. E. Manucharyan *et al.*, Phys. Rev. B **76**, 014524 (2007).
- [5] A. Lupascu *et al.*, Nat. Phys. **3**, 119 (2007).
- [6] I. Katz, A. Retzker, R. Straub, and R. Lifshitz Phys. Rev. Lett. **99**, 040404 (2007).
- [7] V. Peano and M. Thorwart, Chem. Phys. **322**, 135 (2006).
- [8] M. Marthaler and M. I. Dykman, Phys. Rev. A **73**, 042108 (2006).
- [9] M. I. Dykman, Phys. Rev. E **75**, 011101 (2007)
- [10] I. Serban and F. K. Wilhelm, Phys. Rev. Lett. **99**, 137001 (2007).
- [11] M. A. Armen and H. Mabuchi, Phys. Rev. A **73**, 063801 (2006).
- [12] YiJing Yan, Phys. Rev. A **58**, 2721 (1998).
- [13] E. Joos *et al.*, *Decoherence and the Appearance of a Classical World in Quantum Theory* (Springer-Verlag, 2nd Ed., 2003), p. 332.
- [14] C. Stambaugh and H.B. Chan, Phys. Rev. B **73**, 172302 (2006).
- [15] I. Siddiqi, R. Vijay, F. Pierre, C.M. Wilson, M. Metcalfe, C. Rigetti, L. Frunzio, and M.H. Devoret, arXiv:condmat/0312623; I. Siddiqi, R. Vijay, F. Pierre, C.M. Wilson, L. Frunzio, M. Metcalfe, C. Rigetti, and M.H. Devoret, arXiv:cond-mat/0507248.
- [16] L.Z. Guo, Z.G. Zheng, and X.Q. Li, Europhys. Lett. **90**, 10011 (2010).

[1] I. Kozinsky, H. Postma, O. Kogan, A. Husain, and M. Roukes, Phys. Rev. Lett. **99**, 207201(2007).